

Suppressing chaos with mixed superconducting qubit devices

Ben Blain,^{1,2} Giampiero Marchegiani,¹ Luigi Amico,^{1,3,4} and Gianluigi Catelani^{5,1}

¹Quantum Research Center, Technology Innovation Institute, Abu Dhabi 9639, UAE

²School of Physics and Astronomy, University of Kent, Canterbury CT2 7NH, United Kingdom

³Dipartimento di Fisica e Astronomia, Via S. Sofia 64, 95123 Catania, Italy

⁴INFN-Sezione di Catania, Via S. Sofia 64, 95127 Catania, Italy

⁵JARA Institute for Quantum Information (PGI-11),
Forschungszentrum Jülich, 52425 Jülich, Germany

In quantum information processing, a tension between two different tasks occurs: while qubits' states can be preserved by isolating them, quantum gates can be realized only through qubit-qubit interactions. In arrays of qubits, weak coupling leads to states being spatially localized and strong coupling to delocalized states. Here, we study the average energy level spacing and the relative entropy of the distribution of the level spacings (Kullback-Leibler divergence from Poisson and Gaussian Orthogonal Ensemble) to analyze the crossover between localized and delocalized (chaotic) regimes in linear arrays of superconducting qubits. We consider both transmons as well as capacitively shunted flux qubits, which enables us to tune the qubit anharmonicity. Arrays with uniform anharmonicity, comprising only transmons or flux qubits, display remarkably similar dependencies of level statistics on the coupling strength. In systems with alternating anharmonicity, the localized regime is found to be more resilient to the increase in qubit-qubit coupling strength in comparison to arrays with a single qubit type. This result supports designing devices that incorporate different qubit types to achieve higher performances.

Introduction. Superconducting qubits provide a feasible platform for quantum computing and simulation purposes [1]. For computation, fast quantum gates can be attained if the qubits are coupled to each other with sufficient strength [2]. On the other hand, qubits need to be sufficiently isolated to minimize the effects of residual interactions that negatively affect information processing protocols. As such, studying this type of trade-off is a problem of central importance which is attracting considerable attention in the field. It has indeed been argued that qubit arrays for quantum computation should be in a localized regime that can be achieved through a certain amount of spread (disorder) in qubit transition frequencies [3]. Subsequent works showed that quasiperiodic parameter modulation can be more effective than random disorder in keeping the system in the localized regimes [4] and considered the connection to classical chaos in coupled nonlinear oscillators [5]. Fixed qubit-qubit couplings lead to so-called residual ZZ interactions, which can impact gate fidelities in multi-qubit systems [6, 7]. Interestingly enough, such interaction can be suppressed when coupling qubits with opposite anharmonicity [8, 9].

The interplay between localized and extended correlations of qubits also provides a valuable view point for quantum simulation. Specifically, linear arrays of capacitively-coupled transmons [10] have been demonstrated to provide a quantum simulator for driven-dissipative bosonic systems with attractive interactions [11, 12]. In this 1D platform, the many-body localized to ergodic transition has been studied both experimentally and theoretically [13–15], and recently the experimental capabilities have been extended to ladders [16] and 2D arrays [17–20]. In addition, theoretical works have analyzed low-energy states of the system characterized by localized excitations of (bright) solitonic

type [21–23].

In this work we study the localization properties in qubit arrays through the statistical distribution of the energy level spacings of transmons and/or capacitively shunted flux qubits (CSFQs) [24–26]. We employ two different approaches: the first one is based on the average level-spacing ratio, see also Ref. [14]; for the second one we consider a relative entropy of the level spacing distribution known as Kullback–Leibler divergence [3]. Both approaches show that the repulsive (CSFQ) and attractive (transmon) cases are characterized by equivalent spectral statistics, a result that we explain by resorting to an appropriate Bose-Hubbard model. The suppression of unwanted ZZ interactions motivates us to consider arrays with alternating values of anharmonicity, that is, mixed transmon-CSFQ devices; interestingly, we find that the localized phase can persist up to stronger coupling than in arrays with uniform anharmonicity but otherwise identical parameters. We also show that increasing the mismatch between the anharmonicities beyond the value needed for optimal ZZ suppression further stabilizes the localized phase.

Models. An array of M capacitively-coupled qubits is described by the Hamiltonian

$$\hat{\mathcal{H}} = \sum_{i=1}^M \hat{\mathcal{H}}_i^Q + K \sum_{i=1}^{M-1} \hat{N}_i \hat{N}_{i+1}. \quad (1)$$

where $\hat{\mathcal{H}}_i^Q$ is the Hamiltonian of the qubit at site i , either a transmon ($Q = T$) or a CSFQ ($Q = F$), K characterizes the coupling strength between neighboring devices, and \hat{N}_i counts the number of excess Cooper pairs on the island of qubit i . Figure 1(a) schematically shows (top to bottom) transmon and CSFQ arrays, and an array with CSFQs/transmons at odd/even sites.

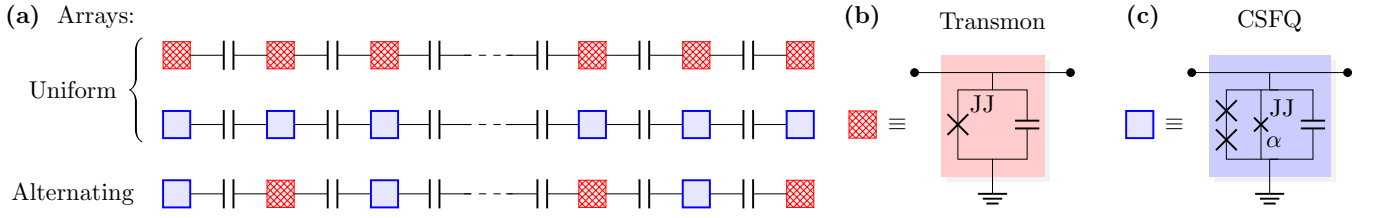


FIG. 1. (a) The systems considered in this work: uniform arrays of transmons (top) and CSFQs (middle), and an array comprising both devices (bottom) with alternating sign anharmonicity. (b) Circuit diagram of a single transmon qubit. (c) Circuit diagram of a single CSFQ. The parameter α represents the ratio of the Josephson energy of the smaller Josephson junction (marked JJ) to the two identical larger Josephson junctions.

The Hamiltonian for the transmon in Fig. 1(b) is [10]

$$\hat{\mathcal{H}}_i^T = 4E_C \hat{N}_i^2 - E_{Ji} \cos \hat{\varphi}_i, \quad (2)$$

where E_C is the charging energy, assumed to be the same for all transmons in an array, E_{Ji} is the Josephson energy, and $\hat{\varphi}_i$, conjugated to \hat{N}_i , is the phase difference across the Josephson junction at site i . We consider the transmon regime $E_{Ji} \gg E_C$, in which the spectrum is weakly anharmonic. The site-index dependence of the Josephson energy can account for variations due to fabrication and/or design choices. For the CSFQ we use the Hamiltonian [26]

$$\hat{\mathcal{H}}_i^F = 4E_{CF} \hat{N}_i^2 + E_{JFi} \{-2 \cos(\hat{\varphi}_i) + \alpha \cos(2\hat{\varphi}_i)\}, \quad (3)$$

where E_{CF} is the charging energy of the CSFQ, E_{JFi} is the Josephson energy of the two identical large junctions of the i^{th} CSFQ, and α is the ratio between the Josephson energy of the third (smaller) Josephson junction and E_{JFi} , see Fig. 1(c). Both E_{CF} and α are taken as independent of i and we have assumed to apply an external magnetic field such that half a flux quantum threads the loop formed by the three junctions. Here $\hat{\varphi}_i$ is a collective variable, the average of the phase differences across the two large junctions, and we ignore the mode associated with the difference of the phases as it has much higher energy [26].

Equation (1) can be approximately cast in the form of a generalized Bose-Hubbard model. Specifically, we introduce bosonic annihilation, \hat{b}_i , and creation, \hat{b}_i^\dagger , operators at each site via the relations $\hat{\varphi}_i = (4A_i)^{-1/4}(\hat{b}_i^\dagger + \hat{b}_i)$ and $\hat{N}_i = \iota(A_i/4)^{1/4}(\hat{b}_i^\dagger - \hat{b}_i)$ [27], where A_i for each qubit type is given in Table I. We then expand the cosines up to the fourth power of $\hat{\varphi}_i$ and for consistency we keep only terms that commute with the number operator $\hat{n}_i = \hat{b}_i^\dagger \hat{b}_i$ (that is, we consider terms up to the next-to-leading order in $\sqrt{1/A_i} \ll 1$). Making a similar approximation in the term coupling neighboring qubits, where we keep the leading terms in $(A_i A_{i+1})^{-1/4}$ that commute with the

	Transmon	CSFQ
A_i	$E_{Ji}/(8E_C)$	$(1 - 2\alpha)E_{JFi}/(4E_{CF})$
ω_{01i}	$\sqrt{8E_{Ji}E_C} - E_C$	$\sqrt{16(1 - 2\alpha)E_{JFi}E_{CF}} - E_{CF} \frac{1-8\alpha}{1-2\alpha}$
U_i	$-E_C$	$E_{CF}(8\alpha - 1)/(1 - 2\alpha)$
$J_{i,i+1}$		$\frac{\kappa}{2} \sqrt[4]{A_i A_{i+1}}$

TABLE I. Relations between the parameters of the qubit array Hamiltonian, Eq. (1), and the Bose-Hubbard one, Eq. (4).

total number operator $\hat{n} = \sum_i \hat{n}_i$, we obtain

$$\begin{aligned} \hat{\mathcal{H}}_{\text{BH}} = & \sum_{i=1}^M \omega_{01i} \hat{n}_i + \sum_{i=1}^M \frac{U_i}{2} \hat{n}_i (\hat{n}_i - 1) \\ & + \sum_{i=1}^{M-1} J_{i,i+1} \left(\hat{b}_{i+1}^\dagger \hat{b}_i + \text{H.c.} \right). \end{aligned} \quad (4)$$

The parameters of the Bose-Hubbard Hamiltonian are related to those of the qubits as in Table I. Note that with our approximations the frequencies ω_{01i} and hopping coefficients $J_{i,i+1}$ depend on the site, while the interaction strengths $U_i = U^Q$ depend only on the qubit type, U^T being always negative for transmons and U^F for CSFQs being positive when $1/8 < \alpha < 1/2$. Note that since $[\hat{\mathcal{H}}_{\text{BH}}, \hat{n}] = 0$, we can subtract a term $\bar{\omega}_{01} \hat{n}$ from the right hand side, where $\bar{\omega}_{01}$ is the average of the frequency over the sites; this shows that the relevant energy scales are the typical fluctuation in the frequency, the interaction energies, and the (average) hopping amplitude.

Level statistics. Studying the statistics of the difference between eigenenergies is a well-established tool to determine whether a system is localized or chaotic. Poisson statistics characterizes localized systems and Wigner-Dyson statistics chaotic ones [28, 29]. Here we consider the distribution $P(r_n)$ of the consecutive level spacing ratio

$$r_n = \min \left\{ \frac{E_{n+1} - E_n}{E_n - E_{n-1}}, \frac{E_n - E_{n-1}}{E_{n+1} - E_n} \right\}, \quad (5)$$

where index $n = 2, \dots, D - 1$ counts the eigenstates in ascending order of energy and D is the dimension of the considered sector of the Hilbert space with a fixed number \mathcal{N} of excitations. By definition, $0 \leq r_n \leq 1$, and,

more importantly for our purposes, the distribution of r_n is independent of the local density of states [30, 31]. The Poisson statistics for energy levels results in the probability distribution for r_n being $P_0(r) = 2/(1+r)^2$. No analytical formulas are in general available for the Wigner-Dyson statistics. Here, since the Hamiltonians have only real entries, we are interested in the distribution for the Gaussian Orthogonal Ensemble (GOE) [32], for which we use the expression

$$P_1(r) = 2C_1 \frac{r + r^2}{[(1+r)^2 - 0.875r]^{5/2}} \quad (6)$$

where $C_1 \simeq 3.662$ is the normalization constant. The subscript $\beta = 0, 1$ in P_β is the so-called Dyson index, denoting the absence ($\beta = 0$) or presence ($\beta > 0$) of level repulsion. The choice of the form of P_1 and its relation to the ‘‘Wigner surmise’’ are discussed in the Supplemental Material (SM) (cf. Ref. [33]).

To quantitatively characterize the crossing point between localization and chaos as we change parameters in the Hamiltonians, we consider two diagnostic tools:

1. the average level spacing ratio $\bar{r} = \sum_n P(r_n)r_n$. The values for the Poisson and GOE distributions are $\bar{r}_0 \simeq 0.3863$ and $\bar{r}_1 \simeq 0.5308$, and we define the crossing point by requiring $\bar{r} = (\bar{r}_0 + \bar{r}_1)/2$;
2. the Kullback-Leibler (KL) divergence D_{KL} ,

$$D_{KL}(P||Q) = \sum_k p_k \log \left(\frac{p_k}{q_k} \right), \quad (7)$$

which gives the entropy of distribution P relative to distribution Q . Here P is the numerically calculated distribution $P(r_n)$, with index k in p_k denoting the k th bin to which the r_n are assigned (see SM for more details on the numerical approach), and Q is either P_0 or P_1 ; the crossing point is identified by requiring $D_{KL}(P||P_0) = D_{KL}(P||P_1)$.

Results. Figure 2 shows the disorder-averaged distribution of r_n for a CSFQ array [Eq. (1) with $Q = F$] for a range of coupling strengths. The distribution nearly follows P_0 (localized) for the lowest coupling considered, $K/h = 1$ MHz, and P_1 (chaotic) for the largest, $K/h = 30$ MHz. With increasing coupling strength, the distributions evolve from P_0 to P_1 . This evolution can be investigated using so-called intermediate statistics [34]; here we only point out that, similarly to the case of transmon arrays [14], we find that the level statistics of the Bose-Hubbard model [Eq. (4)] agrees with that of the CSFQ array, as we show explicitly for one intermediate coupling value.

Now turning to our diagnostic tools, we plot in Fig. 3 the average level spacing and KL divergences for transmon [red curve, $Q = T$ in Eq. (1)], CSFQ (blue curve, $Q = F$), and alternating transmon-CSFQ (green curve, $Q = T/F$ for even/odd site) arrays as a function of the qubit-qubit coupling strength expressed in terms of the (average) hopping amplitude J . The qubit parameters are chosen such that the average frequency $\bar{\omega}_{01}$ as

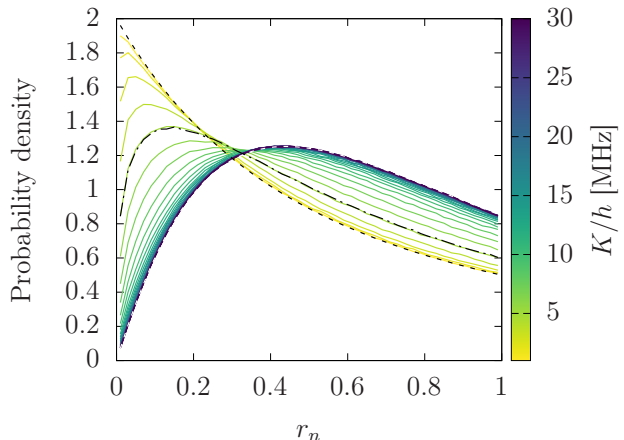


FIG. 2. The distribution of the level spacing ratio r_n [Eq. (5)] for a $M = 10$ CSFQ array (solid lines) with $\mathcal{N} = 5$ excitations for different coupling strengths T in Eq. (1) (color scale). The qubit parameters are $\alpha = 0.35$, $E_{CF}/h = 54$ MHz, and E_{JF} is randomly selected from a Gaussian distribution with mean $E_{JF}/h = 301$ GHz and standard deviation $\delta E_{JF}/h = 8.51$ GHz; these parameters match those of transmon devices [3]. The data is averaged over 5000 disorder realizations. The dashed lines show the distributions P_0 (black) and P_1 (white). The dot-dashed line shows the level statistics for the Bose-Hubbard model [Eq. (4)] with average hopping amplitude J equivalent to $K/h = 5$ MHz.

well as its standard deviation $\delta\omega_{01}$ are the same for all three array types, and the anharmonicities are opposite for transmons and CSFQs, $U^F = -U^T \equiv U$. Both \bar{r} and D_{KL} change smoothly with coupling strength (up to fluctuations whose amplitude decreases by increasing the number of disorder realizations). Clearly, at low coupling all of the distributions are in the localized regime, since $\bar{r} \simeq r_0$ and $D_{KL}(P||P_0) \ll D_{KL}(P||P_1)$, and at large coupling in the chaotic one, $\bar{r} \simeq r_1$ and $D_{KL}(P||P_0) \gg D_{KL}(P||P_1)$.

The transmon and CSFQ arrays display remarkably similar dependencies of \bar{r} and D_{KL} on J (the transmons D_{KL} curves would agree with those in Ref. [3] if plotted with the same normalization). Both quantities are found to be close to the values obtained for the Bose-Hubbard model; this feature reflects a remarkable symmetry that holds for the level statistics of Bose-Hubbard model under the exchange $U \leftrightarrow -U$, if the same disorder distribution symmetric around $\bar{\omega}_{01}$ is used for the two signs of U , see the SM. For all three qubit array types, the crossing points in panel (a) of Fig. 3 (from \bar{r}) are comparable to those in panel (b) (from D_{KL}). This finding cross-validates the two approaches. For concreteness, in what follows we define the crossing point hopping amplitude J_C^Q as the value of J for which the divergences are the same for arrays of type $Q = T, F, A$ (with A denoting arrays with alternating transmon/CSFQ qubits).

The inset in Fig. 3(a) highlights one of our main results, namely that, for disorder strength as in typical

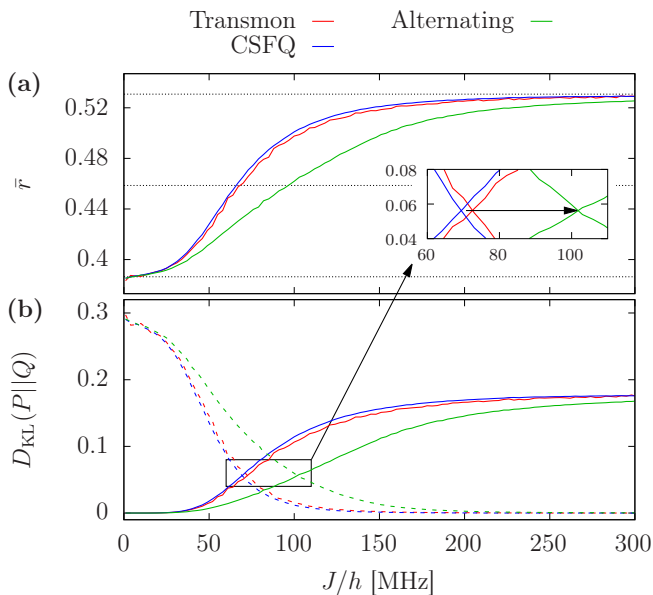


FIG. 3. **(a)** Average level spacing ratio and **(b)** KL divergence for transmon (red), CSFQ (blue), and alternating transmon–CSFQ (green) arrays as functions of average hopping amplitude J . The dotted horizontal lines in panel (a) correspond to (top to bottom) \bar{r}_1 , $(\bar{r}_0 + \bar{r}_1)/2$, and \bar{r}_0 . In panel (b), the solid curves are for $D_{\text{KL}}(P||P_0)$ and the dashed ones for $D_{\text{KL}}(P||P_1)$. Parameters for CSFQs are as in Fig. 2, the corresponding parameters for transmons are $E_C/h = 250$ MHz, $E_J/h = 44$ GHz, $\delta E_J/h = 1.17$ GHz [3]. The inset zooms into the crossing points, highlighting the positive shift in coupling strength for the alternating array when compared to the transmon- and CSFQ-only systems.

devices, the crossing point hopping amplitude is larger for alternating arrays, $J_C^A > J_C^T \simeq J_C^F$. We quantify this enhancement by introducing $\Delta J_C = J_C^A - J_C^F$; in Fig. 4(a) we plot $\Delta J_C/J_C^F$ [calculated for the Bose-Hubbard model, Eq. (4)] as function of $\delta\omega_{01}/U$. The relative enhancement of J_C is largest for weak disorder and decreases monotonically with disorder strength. Such a result can be qualitatively understood by considering the level repulsion between next-nearest-neighbor sites: at small disorder, the fact that the multi-excitation levels of the site placed between the next-nearest-neighbors are detuned due to the opposite sign of U favors localization, but this effect becomes less important with increasing disorder (see SM). In fact, for strong disorder, $\delta\omega_{01}/U \gtrsim 1.7$, we find $J_C^A < J_C^F$, even though for all array types the crossing point hopping increases with disorder, see the inset in Fig. 4(a).

So far we have set $U^T = -U^F$ for the alternating arrays, a choice motivated by the cancellation of ZZ interactions between neighboring qubits [8, 9]. However, from the point of view of localization, we find this is not necessarily the optimal choice. This remarkable feature is highlighted in Fig. 4(b). Indeed, J_C in an alternating array can be increased or decreased by changing the ratio $\eta = -U^F/U^T$. In other words, our results show that

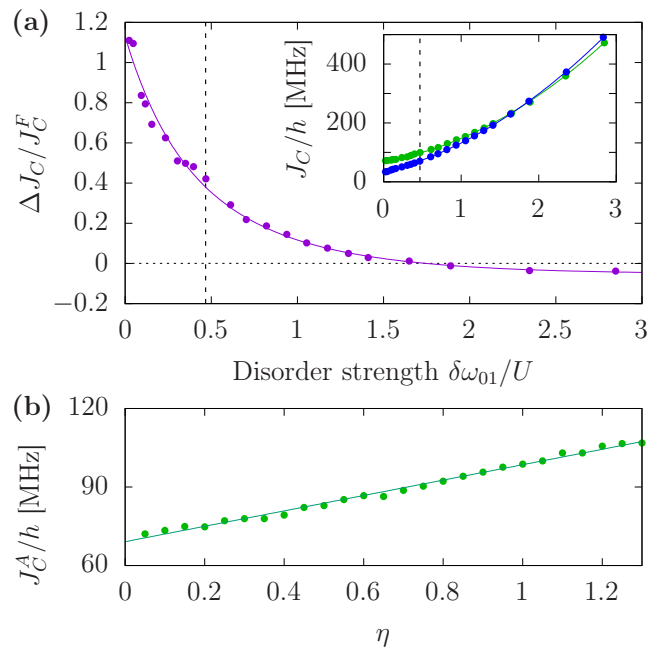


FIG. 4. **(a)** Relative shift in crossing point $\Delta J_C/J_C^F$ as a function of the disorder strength $\delta\omega_{01}/U$ for the Bose-Hubbard model. The dashed vertical line shows the disorder strength used in all other figures (cf. Ref. [3]). The inset shows the numerically calculated values of J_C^F (blue symbols) and J_C^A (green symbols), fitted by quadratic functions (solid curves); the relative difference between those two curves gives the solid line in the main panel. **(b)** Crossing point hopping amplitude J_C^A for an array with alternating transmons and CSFQs vs. ratio of anharmonicities $\eta = -U^F/U^T$ (other parameters as in Fig. 3, mapped to the Bose-Hubbard model according to Table I). The linear best-fit line is shown as a guide to the eye. The points in all panels are obtained by averaging over 1000 disorder realizations.

the localization enhancement in arrays with alternating sign anharmonicity is unrelated to the suppression of the residual ZZ interaction in such systems.

Conclusions. We have investigated the crossover from localized to chaotic regimes in 1D arrays of superconducting qubits comprising C-shunted flux qubits (CSFQ) and transmon qubits displaying positive and negative anharmonicity, respectively, as described by the Hamiltonians in Eqs. (1)-(3). Once the parameters of the models are appropriately matched, the statistics of the level spacing ratio can also be reproduced by using the disordered Bose-Hubbard model of Eq. (4). We note that the level statistics of the Bose-Hubbard model is found to be independent of the sign of the onsite interaction U . Such finding is in contrast with the ground-state properties of the model being clearly different in the attractive or repulsive cases (see [21] and references therein).

Our results indicate that for small disorder strength relative to the anharmonicity, arrays with alternating transmons and CSFQs remain localized up to a higher coupling strength compared with chains consisting of one

qubit type only, see Figs. 3 and 4. Interestingly, the onset of the chaotic behavior arises at even higher coupling when increasing the difference between nearest-neighbor anharmonicities. For disorder strength large compared to the anharmonicity, arrays with a single qubit type or alternating qubits display similar localization properties.

For quantum computing applications, future research could extend our investigation of the localized to chaotic crossover to 2D arrays and/or additional diagnostic tools, such as the Walsh transform [3]. On the quantum sim-

ulation side, the possibility of engineering the strength and nature (attractive/repulsive) of the on-site interaction provides a new platform for the investigation of many-body localization. More broadly, we highlight that superconducting qubits enable tailoring the interaction properties of the system at a *local* level, beyond what has been achieved so far in other platforms, for example the cold atoms one [35, 36].

Acknowledgments. Specialist and High Performance Computing systems provided by Information Services at the University of Kent.

-
- [1] M. Kjaergaard, M. E. Schwartz, J. Braumüller, P. Krantz, J. I.-J. Wang, S. Gustavsson, and W. D. Oliver, Superconducting qubits: Current state of play, *Annu. Rev. Condens. Matter Phys.* **11**, 369 (2020).
- [2] S. Sheldon, E. Magesan, J. M. Chow, and J. M. Gambetta, Procedure for systematically tuning up cross-talk in the cross-resonance gate, *Phys. Rev. A* **93**, 060302 (2016).
- [3] C. Berke, E. Varvelis, S. Trebst, A. Altland, and D. P. DiVincenzo, Transmon platform for quantum computing challenged by chaotic fluctuations, *Nat. Commun.* **13**, 2495 (2022).
- [4] E. Varvelis and D. P. DiVincenzo, Perturbative analysis of quasiperiodic patterning of transmon quantum computers: Enhancement of many-body localization, *Phys. Rev. B* **109**, 144201 (2024).
- [5] S.-D. Börner, C. Berke, D. P. DiVincenzo, S. Trebst, and A. Altland, Classical chaos in quantum computers, *Phys. Rev. Res.* **6**, 033128 (2024).
- [6] D. C. McKay, S. Sheldon, J. A. Smolin, J. M. Chow, and J. M. Gambetta, Three-qubit randomized benchmarking, *Phys. Rev. Lett.* **122**, 200502 (2019).
- [7] E. Magesan and J. M. Gambetta, Effective hamiltonian models of the cross-resonance gate, *Phys. Rev. A* **101**, 052308 (2020).
- [8] J. Ku, X. Xu, M. Brink, D. C. McKay, J. B. Hertzberg, M. H. Ansari, and B. L. T. Plourde, Suppression of unwanted ZZ interactions in a hybrid two-qubit system, *Phys. Rev. Lett.* **125**, 200504 (2020).
- [9] P. Zhao, P. Xu, D. Lan, J. Chu, X. Tan, H. Yu, and Y. Yu, High-contrast ZZ interaction using superconducting qubits with opposite-sign anharmonicity, *Phys. Rev. Lett.* **125**, 200503 (2020).
- [10] J. Koch, T. M. Yu, J. Gambetta, A. A. Houck, D. I. Schuster, J. Majer, A. Blais, M. H. Devoret, S. M. Girvin, and R. J. Schoelkopf, Charge-insensitive qubit design derived from the cooper pair box, *Phys. Rev. A* **76**, 042319 (2007).
- [11] S. Hacoheh-Gourgy, V. V. Ramasesh, C. De Grandi, I. Siddiqi, and S. M. Girvin, Cooling and autonomous feedback in a Bose-Hubbard chain with attractive interactions, *Phys. Rev. Lett.* **115**, 240501 (2015).
- [12] G. P. Fedorov, S. V. Remizov, D. S. Shapiro, W. V. Pogosov, E. Egorova, I. Tsitsilin, M. Andronik, A. A. Dobronosova, I. A. Rodionov, O. V. Astafiev, and A. V. Ustinov, Photon transport in a Bose-Hubbard chain of superconducting artificial atoms, *Phys. Rev. Lett.* **126**, 180503 (2021).
- [13] P. Roushan, C. Neill, J. Tangpanitanon, V. M. Bastidas, A. Megrant, R. Barends, Y. Chen, Z. Chen, B. Chiaro, A. Dunsworth, A. Fowler, B. Foxen, M. Giustina, E. Jeffrey, J. Kelly, E. Lucero, J. Mutus, M. Neeley, C. Quintana, D. Sank, A. Vainsencher, J. Wenner, T. White, H. Neven, D. G. Angelakis, and J. Martinis, Spectroscopic signatures of localization with interacting photons in superconducting qubits, *Science* **358**, 1175 (2017).
- [14] T. Orell, A. A. Michailidis, M. Serbyn, and M. Silveri, Probing the many-body localization phase transition with superconducting circuits, *Phys. Rev. B* **100**, 134504 (2019).
- [15] M. Gong, G. D. de Moraes Neto, C. Zha, Y. Wu, H. Rong, Y. Ye, S. Li, Q. Zhu, S. Wang, Y. Zhao, F. Liang, J. Lin, Y. Xu, C.-Z. Peng, H. Deng, A. Bayat, X. Zhu, and J.-W. Pan, Experimental characterization of the quantum many-body localization transition, *Phys. Rev. Res.* **3**, 033043 (2021).
- [16] Y. Ye, Z.-Y. Ge, Y. Wu, S. Wang, M. Gong, Y.-R. Zhang, Q. Zhu, R. Yang, S. Li, F. Liang, J. Lin, Y. Xu, C. Guo, L. Sun, C. Cheng, N. Ma, Z. Y. Meng, H. Deng, H. Rong, C.-Y. Lu, C.-Z. Peng, H. Fan, X. Zhu, and J.-W. Pan, Propagation and localization of collective excitations on a 24-qubit superconducting processor, *Phys. Rev. Lett.* **123**, 050502 (2019).
- [17] M. Gong, S. Wang, C. Zha, M.-C. Chen, H.-L. Huang, Y. Wu, Q. Zhu, Y. Zhao, S. Li, S. Guo, H. Qian, Y. Ye, F. Chen, C. Ying, J. Yu, D. Fan, D. Wu, H. Su, H. Deng, H. Rong, K. Zhang, S. Cao, J. Lin, Y. Xu, L. Sun, C. Guo, N. Li, F. Liang, V. M. Bastidas, K. Nemoto, W. J. Munro, Y.-H. Huo, C.-Y. Lu, C.-Z. Peng, X. Zhu, and J.-W. Pan, Quantum walks on a programmable two-dimensional 62-qubit superconducting processor, *Science* **372**, 948 (2021).
- [18] J. Braumüller, A. H. Karamlou, Y. Yanay, B. Kannan, D. Kim, M. Kjaergaard, A. Melville, B. M. Niedzielski, Y. Sung, A. Vepsäläinen, R. Winik, J. L. Yoder, T. P. Orlando, S. Gustavsson, C. Tahan, and W. D. Oliver, Probing quantum information propagation with out-of-time-ordered correlators, *Nat. Phys.* **18**, 172 (2022).
- [19] A. H. Karamlou, J. Braumüller, Y. Yanay, A. D. Paolo, P. M. Harrington, B. Kannan, D. Kim, M. Kjaergaard, A. Melville, S. Muschinske, B. M. Niedzielski, A. Vepsäläinen, R. Winik, J. L. Yoder, M. Schwartz, C. Tahan, T. P. Orlando, S. Gustavsson, and W. D. Oliver, Quantum transport and localization in 1d and

- 2d tight-binding lattices, [npj Quantum Inf.](#) **8**, 35 (2022).
- [20] A. H. Karamlou, I. T. Rosen, S. E. Muschinske, C. N. Barrett, A. Di Paolo, L. Ding, P. M. Harrington, M. Hays, R. Das, D. K. Kim, B. M. Niedzielski, M. Schuldt, K. Serniak, M. E. Schwartz, J. L. Yoder, S. Gustavsson, Y. Yanay, J. A. Grover, and W. D. Oliver, Probing entanglement in a 2D hard-core Bose–Hubbard lattice, [Nature](#) **629**, 561 (2024).
- [21] O. Mansikkamäki, S. Laine, and M. Silveri, Phases of the disordered Bose-Hubbard model with attractive interactions, [Phys. Rev. B](#) **103**, L220202 (2021).
- [22] O. Mansikkamäki, S. Laine, A. Piltonen, and M. Silveri, Beyond hard-core bosons in transmon arrays, [PRX Quantum](#) **3**, 040314 (2022).
- [23] B. Blain, G. Marchegiani, J. Polo, G. Catelani, and L. Amico, Soliton versus single-photon quantum dynamics in arrays of superconducting qubits, [Phys. Rev. Res.](#) **5**, 033130 (2023).
- [24] J. Q. You, X. Hu, S. Ashhab, and F. Nori, Low-decoherence flux qubit, [Phys. Rev. B](#) **75**, 140515 (2007).
- [25] M. Steffen, S. Kumar, D. P. DiVincenzo, J. R. Rozen, G. A. Keefe, M. B. Rothwell, and M. B. Ketchen, High-coherence hybrid superconducting qubit, [Phys. Rev. Lett.](#) **105**, 100502 (2010).
- [26] F. Yan, S. Gustavsson, A. Kamal, J. Birenbaum, A. P. Sears, D. Hover, T. J. Gudmundsen, D. Rosenberg, G. Samach, S. Weber, J. L. Yoder, T. P. Orlando, J. Clarke, A. J. Kerman, and W. D. Oliver, The flux qubit revisited to enhance coherence and reproducibility, [Nat. Commun.](#) **7**, 12964 (2016).
- [27] A. Blais, A. L. Grimsmo, S. M. Girvin, and A. Wallraff, Circuit quantum electrodynamics, [Rev. Mod. Phys.](#) **93**, 025005 (2021).
- [28] A. P. Luca D’Alessio, Yariv Kafri and M. Rigol, From quantum chaos and eigenstate thermalization to statistical mechanics and thermodynamics, [Adv. Phys.](#) **65**, 239 (2016).
- [29] D. A. Abanin, E. Altman, I. Bloch, and M. Serbyn, Colloquium: Many-body localization, thermalization, and entanglement, [Rev. Mod. Phys.](#) **91**, 021001 (2019).
- [30] V. Oganesyan and D. A. Huse, Localization of interacting fermions at high temperature, [Phys. Rev. B](#) **75**, 155111 (2007).
- [31] Y. Y. Atas, E. Bogomolny, O. Giraud, and G. Roux, Distribution of the ratio of consecutive level spacings in random matrix ensembles, [Phys. Rev. Lett.](#) **110**, 084101 (2013).
- [32] M. L. Mehta, *Random matrices* (Elsevier, Amsterdam, 2004).
- [33] A. L. Corps and A. Relaño, Distribution of the ratio of consecutive level spacings for different symmetries and degrees of chaos, [Phys. Rev. E](#) **101**, 022222 (2020).
- [34] B. De, P. Sierant, and J. Zakrzewski, On intermediate statistics across many-body localization transition, [J. Phys. A: Math. Theor.](#) **55**, 014001 (2021).
- [35] C. Gross and I. Bloch, Quantum simulations with ultracold atoms in optical lattices, [Science](#) **357**, 995 (2017).
- [36] F. Schäfer, T. Fukuhara, S. Sugawa, Y. Takasu, and Y. Takahashi, Tools for quantum simulation with ultracold atoms in optical lattices, [Nature Reviews Physics](#) **2**, 411 (2020).